Investigation of the fine structure of antihydrogen

M. Ahmadi[1], B.X.R. Alves[2], C.J. Baker[3], W. Bertsche[4,5], A. Capra[6], C. Carruth[7], C.L. Cesar[8], M. Charlton[3], S. Cohen[9], R. Collister[6], S. Eriksson[3], A. Evans[10], N. Evetts[11], J. Fajans[7], T. Friesen[2,10], M.C. Fujiwara[6], D.R. Gill[6], P. Granum[2], J.S. Hangst[2], W.N. Hardy[11], M.E. Hayden[12], E.D. Hunter[7], C.A. Isaac[3], M.A. Johnson[4,5], J.M. Jones[3], S.A. Jones[2,3], S. Jonsell[13], A. Khramov[6,11], P. Knapp[3], L. Kurchaninov[6], N. Madsen[3], D. Maxwell[3], J.T.K. McKenna[6,2], S.Menary[14], J.M. Michan[6,15], T. Momose[11,16], J.J. Munich[12], K. Olchanski[6], A. Olin[6,17] P. Pusa[1], C.Ø. Rasmussen[2], F. Robicheaux[18], R.L. Sacramento[8], M. Sameed[4], E. Sarid[19], D.M. Silveira[8], C. So[10,6], D.M. Starko[14], G. Stutter[2], T.D. Tharp[19], R.I. Thompson[10,6], D.P. van der Werf [3,21], J.S. Wurtele[7]
(The ALPHA Collaboration)

[1] Department of Physics, University of Liverpool, Liverpool L69 7ZE, UK.
[2] Department of Physics and Astronomy, Aarhus University, DK-8000 Aarhus C, Denmark.
[3] Department of Physics, College of Science, Swansea University, Swansea SA2 8PP, UK.
[4] School of Physics and Astronomy, University of Manchester, Manchester M12 9PL, UK.
[5] Cockcroft Institute, Sci-Tech Daresbury, Warrington WA4 4AD, UK.
[6] TRIUMF, 4004 Wesbrook Mall, Vancouver, BC, Canada V6T 2A3.
[7] Department of Physics, University of California at Berkeley, Berkeley, CA 94720-7300, USA.
[8] Instituto de Fisica, Universidade Federal do Rio de Janeiro, Rio de Janeiro 21941-972, Brazil.
[9] Department of Physics, Ben-Gurion University of the Negev, Beer-Sheva 84105, Israel.
[10] Department of Physics and Astronomy, University of Calgary, Calgary AB, Canada T2N 1N4.
[11] Department of Physics and Astronomy, University of British Columbia, Vancouver BC, Canada V6T 1Z1.
[12] Department of Physics, Simon Fraser University, Burnaby BC, Canada V5A 1S6.
[13] Department of Physics, Stockholm University, SE-10691, Stockholm, Sweden.
[14] Department of Physics and Astronomy, York University, Toronto, ON M3J 1P3, Canada.
[15] École Polytechnique Fédérale de Lausanne (EPFL), Swiss Plasma Center (SPC), Lausanne CH-1015, Switzerland.
[16] Department of Chemistry, University of British Columbia, Vancouver BC, Canada V6T 1Z1.
[17] Department of Physics and Astronomy, University of Victoria, Victoria BC, Canada V8P 5C2.
[18] Department of Physics and Astronomy, Purdue University, West Lafayette, Indiana 47907, USA.
[19] Soreq NRC, Yavne, 81800, Israel.
[20] Physics Department, Marquette University, P.O. Box 1881, Milwaukee, WI 53201-1881, USA.
[21] IRFU, CEA/Saclay, F-91191, Gif-sur-Yvette Cedex, France.

At the historic Shelter Island Conference on the Foundations of Quantum Mechanics in 1947, Willis Lamb reported an unexpected feature, a separation of the $2S_{1/2} - 2P_{1/2}$ states, in the fine structure of the atomic hydrogen spectrum [1]. The observation of this separation, now known as the Lamb shift, marked an important event in the evolution of modern physics, inspiring Tomonaga, Schwinger, Feynman and others to develop a renormalizable theory of quantum electrodynamics (QED) [2, 3, 4, 5]. Here we report measurements of the fine structure in the n=2 states of antihydrogen, the antimatter

counterpart of the hydrogen atom. By optical excitation of the 1*S*-2*P* Lyman-α transitions in antihydrogen [6], we determine their frequencies in a magnetic field of 1 T to a precision of 16 parts per billion. By assuming the standard Zeeman and hyperfine interactions, we can infer the zero-field fine structure splitting ($2P_{1/2}$–$2P_{3/2}$) in antihydrogen. The resulting value is consistent with the predictions of QED at the 2% level of precision. Using our previously measured value of the 1*S*-2*S* transition frequency [7], we find that the $2S_{1/2}$-$2P_{1/2}$ splitting is consistent with theory at the level of 11%. Our observations represent an important step towards precision measurements of the fine structure in the antihydrogen spectrum as tests of charge-parity-time (CPT) symmetry [8], and towards the determination of other fundamental quantities, such as the Lamb shift and the antiproton charge radius [9, 10], in this antimatter system.

In the expected energy levels of antihydrogen in the n=2 states (Fig. 1), the splitting of the 2P state into two states ($2P_{3/2}$ and $2P_{1/2}$) at zero magnetic field is called the fine structure splitting. This splitting, predicted by the Dirac theory of relativistic quantum mechanics for normal hydrogen [11], originates from the spin-orbit interaction between the non-zero orbital angular momentum (L=1) and the positron spin. The Lamb shift was originally defined as the splitting between the $2S_{1/2}$ and $2P_{1/2}$ states at zero field, and is a manifestation of the interaction of the electron with the quantum fluctuations of the vacuum electromagnetic field, an effect explained by QED [12, 13, 14]. Today, it is understood that the historical Lamb shift is dominated by the QED effects on the 2S energy level, which we have recently addressed in antihydrogen [7].

In non-zero magnetic fields, the Zeeman effect causes the $2P_{3/2}$ state to also split into four sublevels (labelled $2P_a$, $2P_b$, $2P_c$, and $2P_d$ in Fig. 1), while the $2S_{1/2}$ and $2P_{1/2}$ states each split into two ($2S_{ab}$, $2S_{cd}$ and $2P_e$, $2P_f$). These fine structure levels further split into two hyperfine states each due to the antiproton spin (see the Fig. 1 caption for the notation for the energy levels).

Lamb's original work used the then newly-developed techniques of an excited-state atomic hydrogen beam and resonant microwave spectroscopy to study direct transitions between the n=2 fine structure states in various magnetic fields. The Lamb shift was then determined to 10% precision by extrapolating frequency measurements to zero field [1]. Here, we report the observation of the splitting between the $2P_c$ and $2P_f$ states in antihydrogen in a field of 1 T, by studying laser-induced transitions from the ground state. These studies have become possible due to the combination of several recent advances: the accumulation [15] of hundreds of anti-atoms for each run, their confinement for many hours [16], control of the hyperfine polarisation of the antihydrogen samples [17], and the development of a narrow-line, pulsed, Lyman-alpha laser [6, 18].

Details of production, trapping, and control of antihydrogen in the ALPHA experiment have been described elsewhere [6, 7, 15-25], so the description given here is brief. The ALPHA-2 apparatus (Fig. 2) incorporates a cylindrical magnetic trapping volume (about 400 cm^3) for neutral anti-atoms; the magnetic field minimum at the centre of the trap was set to 1.0329 ±0.0004 T for this work. By combining 90,000 antiprotons trapped from the CERN Antiproton Decelerator [23] and three million positrons from a positron accumulator [24, 25], about 10 - 30 cold (below 0.54 K) anti-atoms are confined in the magnetic trap in a

4-minute cycle. Under normal conditions, the storage lifetime of the trapped antihydrogen is greater than 60 hours [16], which permits loading from repeated cycles [15] to obtain hundreds of antihydrogen atoms in a few hours.

Two types of antihydrogen samples were used in these studies. The positron spin of an antihydrogen atom confined in the ALPHA-2 trap is necessarily polarized, since only the $1S_c$ and $1S_d$ states can be magnetically trapped (Fig. 1). The antiproton spin, on the other hand, is unpolarized *a priori*, with both orientations equally likely. Thus, the initial samples are *singly spin-polarized*. On the other hand, *doubly spin-polarized* samples, in which both the positron and antiproton spins are polarized, can be prepared by injecting microwaves to resonantly drive the $1S_c$ atoms to the untrappable $1S_b$ state (Fig. 1), effectively depopulating the $1S_c$ state from the trap [17].

Spectroscopy in the VUV (vacuum ultraviolet) range is challenging even for ordinary atoms, due in part to the lack of convenient laser sources and optical components [26, 27, 28]. Our pulsed, coherent, 121.6 nm radiation was produced by generating the third harmonic of 365 nm pulses in a Kr/Ar gas mixture at a repetition rate of 10 Hz [18]. The typical pulse width at 121.6 nm was 12 ns, and the bandwidth was estimated, from the Fourier transform of the temporal pulse shape, to be 65 MHz (full-width at half-maximum, FWHM). The 121.6 nm light was linearly polarized because of the three-photon mixing of linearly polarized 365 nm light. In the antihydrogen trap, the polarization vector is nearly perpendicular to the direction of the axial magnetic field. The laser had a beam radius of 3.6 mm, roughly collimated across the trapping region (Fig. 2). The average pulse energies in the antihydrogen trapping volume ranged from 0.44 nJ to 0.72 nJ over different runs, as evaluated

from the pulse waveforms recorded with a calibrated, solar-blind photomultiplier detector.

In this experiment, single-photon transitions from the $1S_c$ ($1S_d$) states to the $2P_{c+}$ ($2P_{c-}$) and $2P_{f+}$ ($2P_{f-}$) states are driven by the 121.6 nm light (red and blue arrows in Fig. 1). When antihydrogen is excited to the $2P_{c\pm}$ or $2P_{f\pm}$ state, it decays to the ground state manifold within a few ns by emitting a photon at 121.6 nm. The mixed nature of the positron spin states in the $2P_{c+}$ ($2P_{c-}$) and $2P_{f+}$ ($2P_{f-}$) states implies that these states can decay to the $1S_b$ ($1S_a$) states via a positron spin flip (black dashed arrows in Fig. 1). Atoms in these final states are expelled from the trap, resulting in their annihilations on the trap walls. Annihilation products (charged pions) are in turn detected by a silicon vertex detector [29] with an efficiency greater than 80%.

Table 1 summarizes our data. In total, four series of measurements were performed using either singly or doubly spin-polarized samples. The Series 1 data, previously reported in ref [6], have been reanalyzed. Each series consisted of two or four runs, and for each run, about 500 antihydrogen atoms were accumulated over approximately two hours, typically involving over 30 production cycles. The trapped anti-atoms were then irradiated for about two hours by a total of 72,000 laser pulses at twelve different frequencies (i.e. 6,000 pulses per frequency point for each run) spanning the range -3.10 GHz to +2.12 GHz relative to the expected (hydrogen) transition frequencies. The laser frequency was changed every 20 s in a non-monotonic fashion in order to minimize effects related to the depletion of the sample of antihydrogen. After the laser exposure, the remaining antihydrogen atoms were released by shutting down the trap magnets, typically in 15 s, and counted via detection of their annihilation events. Some 40 - 60% of the trapped

antihydrogen atoms experienced resonant, laser-induced spin flips, and their annihilations were detected during the two-hour laser irradiation period.

A combination of time-gated antihydrogen detection (enabled by the use of a pulsed laser), the accumulation of a large number of anti-atoms, and the use of a supervised machine-learning analysis [29] (based on a boosted decision tree classifier) suppressed the background in the current experiments to a negligible level (less than 2 counts per 2-hour irradiation period).

The measured spectra, obtained from counting the laser-induced spin flip events, are shown in Fig. 3 for both singly spin-polarized and doubly spin-polarized antihydrogen samples. For each run, the probability at each frequency point is determined from dividing the number of annihilation events recorded at that frequency by the total number of trapped atoms in that run, and further dividing by the ratio of the average laser energy to a standard value of 0.5 nJ. The normalization to the standard laser energy is to account for the expected linear dependence of transition probability on laser power in our regime. The data plotted in Fig. 3 are spectrum averaged over the runs for each series. For the singly polarized sample (Fig. 3(a)), each transition shows a linewidth of about 1.5 GHz (FWHM). This is consistent with the expected Doppler broadening in our trapping condition (1 GHz, FWHM) and the hyperfine splitting of the $1S - 2P_f$ and $1S - 2P_c$ transitions (0.71 GHz for both transitions). The hyperfine structure cannot be resolved in these singly polarized samples due to the Doppler broadening.

Figure 3(b) shows the spectra obtained from doubly spin-polarized antihydrogen samples. For these data, ~28 GHz microwave radiation (power ~ 0.4 W, measured at the trap entrance) was applied before the

start of optical spectroscopy, in the form of a 9 MHz sweep, covering the $1S_c - 1S_b$ transition in the magnetic field minimum [17]. As shown in Table 1, about half of the total trapped antihydrogen atoms underwent a positron spin flip and annihilated during microwave irradiation. This is consistent with our experience from earlier studies in which $1S_c$ state atoms are removed with about 95% efficiency [7, 17]. The spectral lines of the $1S$-$2P$ transitions in doubly spin-polarized antihydrogen (Fig. 3b) are narrower, relative to those in the singly spin-polarized samples (Fig. 3a), since the former involves only one hyperfine state in the ground state. The peaks are red-shifted because the frequencies of the transition from the $1S_d$ state to the $2P_f$ and $2P_c$ states are expected to be about 700 MHz lower than those from the $1S_c$ state. The observed ~1 GHz FWHM of these lines is in agreement with the Doppler width expected for our trapping conditions.

The procedure used to extract the frequencies of the fine structure transitions and to evaluate their associated uncertainties is described in Methods. We summarize the results of this analysis in Table 2. A simulation was used to model the motion of trapped antihydrogen atoms in the ALPHA-2 trap and their interaction with pulsed laser radiation. The resonant transition frequencies were obtained by comparing simulated and experimental lineshapes. Extensive investigations were performed to evaluate systematic uncertainties in our measurement (Table 3). The validity of our analysis procedure was tested by using different lineshape fitting models. Two representative curve fits are shown in Fig. 3. The Model 1 fit is to a function constrained to fit the simulation shape, while in Model 2 the shape parameters of this function are allowed to vary to best fit the experimental data - see Methods for details. Sensitivity of the results to experimental and simulation parameters was tested by repeating

the analysis procedure for a number of simulations with varied input. These included initial antihydrogen conditions (such as the initial temperature, the quantum state, and the cloud diameter of antihydrogen at formation), and laser properties (such as linewidth, beam waist size, and beam position). See Methods and Extended Data, Fig. 1. Other sources of systematic uncertainties include the calibration accuracy and a possible frequency drift of the wavemeter, frequency shifts of the 730 nm amplification laser cavity, and the possible incomplete clearing of the $1S_c$ state in doubly spin-polarized sample preparation (Table 3 and Methods).

Within the uncertainties, the measured transition frequencies agree with theoretical expectations for hydrogen for all four series (Table 2 and Fig. 4). The fact that the four measurements are consistent, despite having different systematics, increases the confidence in our overall results. The results can be combined to give a test of CPT invariance in the $1S - 2P$ transitions at the level of 16 parts per billion (Fig. 4).

Fundamental physical quantities in antihydrogen can be extracted from our optical measurements of the $1S - 2P$ transitions by combining them with our earlier measurement of the $1S - 2S$ transition at the same magnetic trapping field [7]. From the weighted average of the results between the singly polarized and doubly polarized measurements (Table 1), we obtain a $2P_{c-} - 2\ P_{f-}$ splitting of 14.945 ± 0.075 GHz, a $2S_d - 2P_{c-}$ splitting of 9.832 ± 0.049 GHz and a $2S_d - 2P_{f-}$ splitting of 24.778 ± 0.060 GHz at 1.0329 T (Methods). Only two out of the three splittings are independent, and they all agree with the values predicted for normal hydrogen in the same field. In interpreting our data, we categorize features in the spectrum based on the order of the fine structure constant α in a perturbative series expansion in quantum field theory. Those features that can be described by the Dirac theory (the Zeeman, hyperfine, and

fine structure effects) are referred to as the tree-level effects, and follow from the lower order terms (up to order ~$\alpha^2 Ry$, where Ry is the Rydberg constant). On the other hand, the Lamb shift originates from the so-called loop effects (order ~$\alpha^3 Ry$), whose calculation requires the concept of renormalization to avoid infinities [12, 13, 14]. Each of the measured splittings has different sensitivity to different terms. At the level of our precision, the $2P_c - 2P_f$ splitting is sensitive to the tree-level terms with negligible QED effects, while the $2S - 2P_f$ and $2S - 2P_c$ splittings are sensitive to the field-independent Lamb shift, in addition to the tree-level terms (note that the Lamb shift is predicted to have negligible dependence on magnetic field). The agreement between our measurement and the Dirac prediction for the $2P_{c-} - 2P_{f-}$ splitting supports the consistency of the tree-level theory in describing the Zeeman, hyperfine and fine structure interactions in the $2P$ states of antihydrogen. If we hence assume that we can correctly account for the tree-level effects in our measurements, we can infer from our measured splittings the values of the zero-field fine structure splitting in antihydrogen to be 10.88 ± 0.19 GHz. Combining the current result with the much more precisely measured 1S-2S transition frequency in antihydrogen [7], we obtain a Lamb shift of 0.99 ± 0.11 GHz (Methods). Again, most of the expected physical effect is on the 2S level, so we should consider this value to represent a proof of principle of the necessary experimental techniques. If we use the theoretical value of the fine structure splitting from the Dirac prediction (rather than treat it as a parameter), we can derive a tighter constraint on the Lamb shift, 1.046 ± 0.035 GHz.

When considering the first measurements on an exotic system like antihydrogen, it is necessary to adopt a framework within which it is possible to compare the results to the expectations of well-established

models for normal matter. The choice of which effects can be assumed to be true in interpreting this data is, of necessity, somewhat arbitrary. The approach illustrated here is based on the order of perturbation in the coupling constant α; we have assumed (lower order) tree-level effects, in order to extract (higher order) renormalizable loop effects. Other approaches are possible in interpreting our data.

We have investigated the fine structure of the antihydrogen atom in the n=2 states. The splitting between $2P_c$ and $2P_f$ states, two of the $2P$ Zeeman sub-levels belonging to the $J=3/2$ and $J=1/2$ manifolds, have been observed in a magnetic field of 1 T. The energy levels of the $1S$-$2P$ transitions agree with the Dirac theory predictions for hydrogen in 1 T to 16 parts per billion, and their difference to 0.5 %. By assuming the standard Zeeman and hyperfine effects, and by combining our results with the earlier result of 1S-2S spectroscopy [7], we have inferred the zero-field fine structure splitting and the Lamb shift.

These observations expand the horizons of antihydrogen studies, providing opportunities for precision measurements of the fine structure and the Lamb shift, both longstanding goals in the field. Prospects exist for significant improvements in the precision beyond this initial determination. With the advent of the ELENA ring, an upgrade to the AD with an anticipated increase in the antiproton flux, the statistical uncertainties should be dramatically reduced. The development of laser cooling [30] should reduce the Doppler width to the level comparable to the natural linewidth, which in turn would improve the precision of the frequency determination. It would also permit direct experimental determination of the hyperfine splitting in the $2P$ states, for which theoretical values were assumed in this study. Such measurements will provide tests of CPT invariance that are complementary to other precision

measurements in antihydrogen such as the 1S-2S and the ground state hyperfine transitions. Furthermore, a precise value of the Lamb shift, combined with that of the 1S-2S interval, will permit an antimatter-only determination of the antiproton charge radius [9, 10], without referring to the measurements in the matter sector, *i.e.*, independent of the current puzzle in the proton charge radius [31, 32, 33]. These examples signify the importance of broad and complementary measurements in testing fundamental symmetries of Nature. In the absence of compelling theoretical arguments to guide the way to possible asymmetries, it is essential to address the antihydrogen spectrum as comprehensively as is practical. Finally, the results reported here demonstrate our capability to precisely and reproducibly drive VUV transitions on a few anti-atoms, and indicate our readiness for laser cooling of antihydrogen [30], an eagerly anticipated development in antimatter studies with far-reaching implications.

References:

[1] Lamb, W.E. Jr. & Retherford, R.C. Fine structure of the hydrogen atom by a microwave method. *Phys. Rev.* **72**, 241-243 (1947).
[2] Tomonaga, S. On a relativistically invariant formulation of the quantum theory of wave fields. *Prog. Theo. Phys.* **1**, 27-42 (1946).
[3] Schwinger, J. On quantum-electrodynamics and the magnetic moment of the electron. *Phys. Rev.* **73**, 416-417 (1948).
[4] Feynman, R. P. Space–time approach to quantum electrodynamics. *Phys. Rev*. **76**, 769-789 (1949).
[5] See for a fascinating historical account: QED and the men who made it: Dyson, Feynman, Schwinger, and Tomonaga. Schweber, S.S. (Princeton University Press, 1994).
[6] Ahmadi M. et. al., Observation of the 1S-2P Lyman-alpha transition in antihydrogen. *Nature* **561**, 211-215 (2018).
[7] Ahmadi, M. et. al., Characterization of the 1S–2S transition in antihydrogen. *Nature* **557**, 71-75 (2018).
[8] Kostelecky, V. A. & Vargas, A. J. Lorentz and CPT tests with hydrogen, antihydrogen, and related systems. *Phys. Rev.* D **92**, 056002 (2015).
[9] Crivelli, P., Cooke, D. & Heiss, M. W. Antiproton charge radius, *Phys. Rev.* D **94**, 052008 (2016).
[10] Eriksson, S., Precision measurements on trapped antihydrogen in the ALPHA experiment. *Philosophical Transactions of the Royal Society A: Mathematical, Physical and Engineering Sciences* vol. 376 p. 2017.0268 (2018).
[11] Dirac, P.A.M. The quantum theory of the electron. *Proc. R. Soc. Lond.* A**117**, 610-624 (1928).
[12] Quantum Electrodynamics. Ed. Kinoshita, T., World Scientific, Singapore, (1990).

[13] Karshenboim, S.G. Precision physics of simple atoms: QED tests, nuclear structure and fundamental constants. *Phys. Rep.* **422**, 1-63 (2005).
[14] Brodsky, S. J. & Parsons, R. G. Precise theory of the Zeeman spectrum for atomic hydrogen and deuterium and the Lamb shift. Phys. Rev. 163, 134-146 (1967).
[15] Ahmadi, M. et al. Antihydrogen accumulation for fundamental symmetry tests. *Nature Communications* **8**, 681 (2017).
[16] Capra, A. & ALPHA Collaboration. Lifetime of magnetically trapped antihydrogen in ALPHA. *Hyperfine Interact*. 240, 9 (2019).
[17] Ahmadi, M. et. al. Observation of the hyperfine spectrum of antihydrogen, *Nature* **548**, 66-69 (2017).
[18] Michan, J. M., Polovy, G., Madison, K. W., Fujiwara, M. C. & Momose, T. Narrowband solid state VUV coherent source for laser cooling of antihydrogen. *Hyperfine Interact*. **235**, 29–36 (2015).
[19] Andresen, G. B. et al. Trapped antihydrogen. *Nature* **468**, 673–676 (2010).
[20] Andresen, G. B. et al. Confinement of antihydrogen for 1000 seconds. *Nature Physics* **7**, 558–564 (2011).
[21] Ahmadi, M. et al. Observation of the 1S–2S transition in trapped antihydrogen. *Nature* **541**, 506–510 (2017).
[22] Ahmadi, M. et al. Enhanced control and reproducibility of non-neutral plasmas. *Phys. Rev. Lett*. **120**, 025001 (2018).
[23] Maury, S. The antiproton decelerator: AD. *Hyperfine Interact.* **109**, 43–52 (1997).
[24] Murphy, T. J. & Surko, C. M. Positron trapping in an electrostatic well by inelastic collisions with nitrogen molecules. *Phys. Rev. A* **46**, 5696–5705 (1992).
[25] Surko, C. M., Greaves, R. G. & Charlton, M. Stored positrons for antihydrogen production. *Hyperfine Interact.* **109**, 181–188 (1997).
[26] Luiten, O.J. et al. Lyman-α spectroscopy of magnetically trapped atomic hydrogen, *Phys. Rev. Lett*. **70**, 544-547 (1993).
[27] Eikema, K. S. E., Walz, J. & Hänsch, T. W. Continuous coherent Lyman- α excitation of atomic hydrogen. *Phys. Rev. Lett*. **86**, 5679 – 5682 (2001).
[28] Gabrielse, G. et al. Lyman-α source for laser cooling antihydrogen, *Opt. Lett*. **43**, 2905-2908 (2018).
[29] Stracka, S. Real-time detection of antihydrogen annihilations and applications to spectroscopy. EPJ. Conf. 71, 00126 (2014).
[30] Donnan, P. H., Fujiwara, M. C. & Robicheaux, F. A proposal for laser cooling antihydrogen atoms. *J. Phys*. B **46**, 025302 (2013).
[31] Pohl, R. et al. The size of the proton. *Nature* **466**, 213-216 (2010).
[32] Beyer, A. et al. The Rydberg constant and proton size from atomic hydrogen. *Science* **357**, 68-75 (2017).
[33] Fleurbaey, H et al. New measurement of the transition frequency of hydrogen: contribution to the proton charge radius puzzle. *Phys. Rev. Lett*. **120**, 183001 (2018).

Acknowledgements This work was supported by: the European Research Council through its Advanced Grant programme (JSH); CNPq, FAPERJ, RENAFAE (Brazil); NSERC, ALPHA-g/CRUCS CFI, NRC/TRIUMF, EHPDS/EHDRS (Canada); FNU (Nice Centre), Carlsberg Foundation (Denmark); ISF (Israel); STFC, EPSRC, the Royal Society and the Leverhulme Trust (UK); DOE, NSF (USA); and VR (Sweden). We are grateful for the efforts of the CERN AD team, without which these experiments could not have taken place. We thank Pavle Djuricanin (University of British Columbia) for his extensive help with the laser system and calibrations. We

thank Jacky Tonoli (CERN) and his staff as well as Tony Mittertreiner (UBC) and his staff for extensive, time-critical help with machining and electrical works. We thank the staff of the Superconducting Magnet Division at Brookhaven National Laboratory for collaboration and fabrication of the trapping magnets. We thank C. Marshall (TRIUMF) for his work on the ALPHA-2 cryostat. We thank Professor F. Besenbacher (Aarhus) for timely support in procuring the ALPHA-2 external solenoid. We thank Professor T. Miller (Ohio) for advice on the initial development of the pulsed laser system. We thank Professors A. Kostelecky and G. Drake for discussions on the theoretical aspects of this work.

Author Contributions This experiment was based on data collected using the ALPHA-2 antihydrogen trapping apparatus, designed and constructed by the ALPHA Collaboration using methods developed by the entire collaboration. The entire collaboration participated in the operation of the apparatus and the data taking activities. Pulsed Lyman alpha spectroscopy was first proposed by MCF and developed further by TM, FR, JMM, RAC, AE, AK and MCF. The original laser was designed by TM and tested by JMM, PD and TM. The laser system at CERN was implemented, commissioned and operated by JMM, RAC, AE, AK and TM. FR has developed the simulation program for laser interaction with magnetically trapped atoms. Microwave techniques and ECR magnetometry were developed by TF, MEH and WH. The positron accumulator is the responsibility of CJB, MC, MS, CAI and DPvdW. The annihilation detector system was developed by AC, MCF, DRG, LK, JTKM, SM, KO, AO, and PP. Detailed analysis of the antiproton annihilation detector data was done by JTKM, AE and AO. The frequency determination and the evaluation of its uncertainty was performed by TM, MCF, AK, AE, RAC, RIT and AO. The manuscript was written by TM, MCF and JSH, with significant input from AK, RAC, AE, AO, JTKM, MH, and FR. The manuscript was then edited and improved by the entire collaboration.

Author Information Reprints and permissions information is available at www.nature.com/reprints. The authors declare no competing financial interests. Readers are welcome to comment on the online version of the paper. Correspondence

and requests for materials should be addressed to TM (momose@chem.ubc.ca), MCF (Makoto.Fujiwara@triumf.ca), or JSH (jeffrey.hangst@cern.ch).

Data availability statement The datasets generated during and/or analysed during the current study are available from the corresponding author (jeffrey.hangst@cern.ch) on reasonable request.

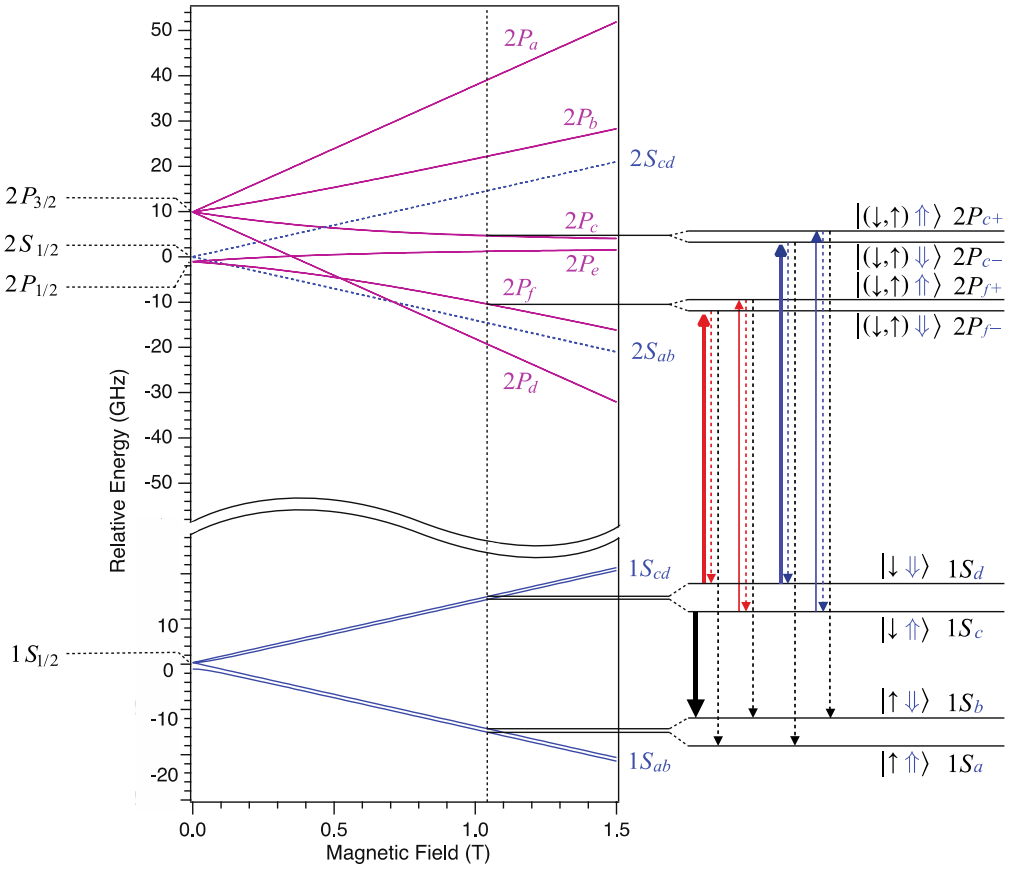
$2P_a$
$2P_b$
$2S_{cd}$
$2P_c$
$2P_e$
$2P_f$
$2S_{ab}$
$2P_d$
$1S_{cd}$
$1S_{ab}$
$2P_{3/2}$
$2S_{1/2}$
$2P_{1/2}$
$1S_{1/2}$
Relative Energy (GHz)
Magnetic Field (T)
$|(\downarrow,\uparrow)\Uparrow\rangle\ 2P_{c+}$
$|(\downarrow,\uparrow)\Downarrow\rangle\ 2P_{c-}$
$|(\downarrow,\uparrow)\Uparrow\rangle\ 2P_{f+}$
$|(\downarrow,\uparrow)\Downarrow\rangle\ 2P_{f-}$
$|\downarrow\Downarrow\rangle\ 1S_d$
$|\downarrow\Uparrow\rangle\ 1S_c$
$|\uparrow\Downarrow\rangle\ 1S_b$
$|\uparrow\Uparrow\rangle\ 1S_a$

Figure 1: **Expected antihydrogen energy levels.** Calculated energies of the fine structure and the hyperfine sublevels of the $1S_{1/2}$, $2S_{1/2}$, $2P_{3/2}$ and $2P_{1/2}$ states are shown as functions of magnetic field strength. The spin orientations for antihydrogen are shown; they are reversed for hydrogen. The centroid energy difference, $E_{1S\text{-}2S}$ $=2.4661\times10^{15}$ Hz, has been suppressed on the vertical axis. Details of the energy levels relevant to this work at the field of B=1.0329 T are shown on the right of the figure. Each state is labeled based on the conventional notations. For the 1S and 2S states, the hyperfine states are labeled with subscripts a to d in order of *increasing* energy (see e.g. [7]), namely $S_a=|\uparrow\Uparrow\rangle$, $S_b=|\uparrow\Downarrow\rangle$, $S_c=|\downarrow\Uparrow\rangle$, and $S_d=|\downarrow\Downarrow\rangle$, where the ket notation represents the positron spin (left; $\downarrow$ or $\uparrow$) and antiproton spin (right; $\Downarrow$ or $\Uparrow$) states in the high-field limit. The labels S_{ab} and S_{cd} are used when the antiproton spins are unpolarized. On the other hand, for the 2P states, the fine structure splittings are labeled with subscripts a through f in order of *decreasing* energy at low magnetic fields, while the hyperfine splitting due to the antiproton spin is specified by subscripts + and – for the spin parallel ($\Uparrow$) and anti-parallel ($\Downarrow$) to the magnetic field in the high-field limit, respectively. The symbol ($\downarrow$,$\uparrow$) in the figure indicates that the positron spin states are mixed for the $2P_c$ and $2P_f$ states. The vertical solid arrows indicate the one-photon laser transitions probed here for the $1S_d \rightarrow 2P_{f-}$ (bold red), $1S_c \rightarrow 2P_{f+}$ (thin red), $1S_d \rightarrow 2P_{c-}$ (bold blue), and $1S_c \rightarrow 2P_{c+}$ (thin blue). The broken red and blue arrows indicate relaxation to the same trappable level, which is not detectable in the present experiment, while the broken black arrows indicate relaxation to untrappable levels, which is detectable via annihilation signals (see text). The bold black arrow shows the microwave transition used to eliminate $1S_c$ state atoms to prepare a doubly spin-polarized antihydrogen sample.

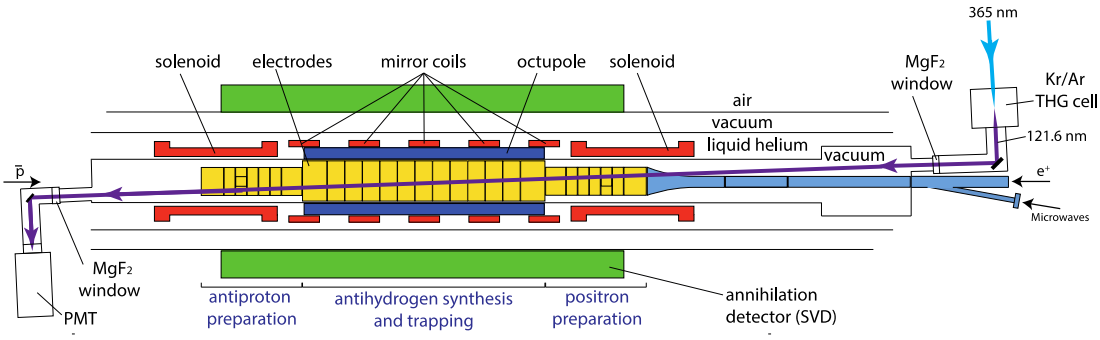

Figure 2: The ALPHA-2 central apparatus.

A cylindrical trapping volume for neutral antimatter with a diameter of 44.35 mm and an axial length of 280 mm is located inside several Penning trap electrodes and surrounded by an octupole coil, five mirror coils, and two solenoids, all superconducting. The three-layer silicon vertex annihilation detector is shown schematically in green. Laser light (purple line) enters from the positron (e^+) side (right) and is transmitted to the antiproton ($\bar{p}$) side (left) through vacuum-ultraviolet-grade MgF_2 ultrahigh-vacuum windows. The laser beam crosses the trap axis at an angle of 2.3°. The transmitted 121.6 nm pulses are detected by a solar-blind photomultiplier tube (PMT) at the antiproton side. Microwaves to prepare the doubly spin-polarized samples are introduced from the positron side through a waveguide, shown in blue. The external solenoid magnet for the Penning traps is not shown here.

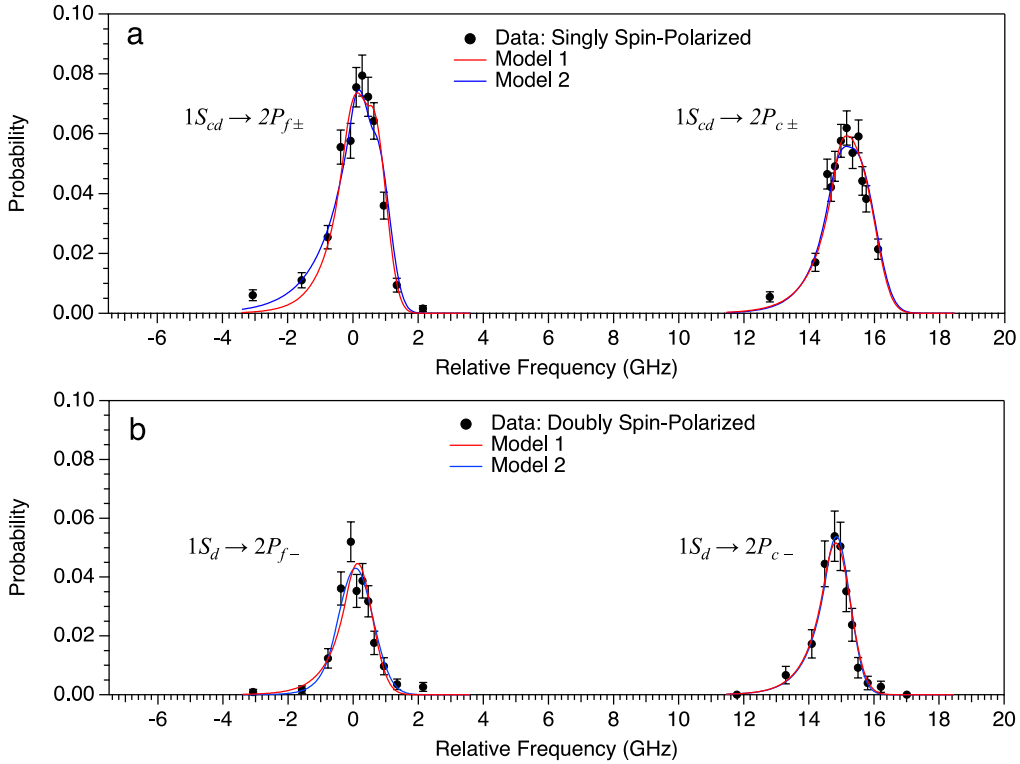

Figure 3: **1*S*-2*P* fine structure spectrum of antihydrogen.**

Experimental data (filled circles with error bars) and fitted lineshapes are plotted for (a) singly spin-polarized and (b) doubly spin-polarized antihydrogen samples. The data points were obtained from the detected spin flip events, normalized to the total number of trapped antihydrogen atoms and a laser pulse energy of 0.5 nJ. The error bars are 1-s.d. counting uncertainties. The frequency is offset by 2,466,036.3 GHz. Note that no data were taken between the two peaks (between ~ 2 -12 GHz). Red fit curves are obtained via our standard fit procedure (Model 1), while blue curves are derived from an alternative fit model (Model 2), illustrating the sensitivity of our results to fit procedures. See text and Methods for detailed discussion.

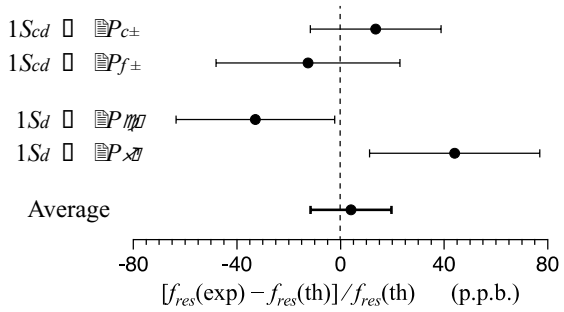

Figure 4: **Comparison of the antihydrogen and hydrogen transition frequencies.**

The experimentally measured frequencies for the 1*S*-2*P* transitions in antihydrogen f_{res}(exp) are compared with those theoretically expected for normal hydrogen f_{res}(th) (Table 2). All four measurements are consistent with normal hydrogen, and their average gives a combined test of CPT invariance at the 16 p.p.b. (parts per billion) level. The error bars are one standard deviation, and the error bar for the average takes into account correlated uncertainties. (Methods).

Table 1: Experimental parameters and number of detected events.

The experimental parameters together with the number of antihydrogen events detected during the microwave irradiation, laser irradiation and during the release of remaining atoms, are tabulated for each series. The machine-learning analysis identifies annihilation events with an estimated efficiency of 0.849 for the microwave irradiation, 0.807 for the laser irradiation, and 0.851 for the release of the remaining atoms. The counts are corrected for the detection efficiencies. The number of trapped atoms is derived from the sum of the other counts.

Series	Sample polarization	Transition probed	№ runs	Pulse energy (pJ, avg.)	№ freq.	№ pulses per freq.	№ trapped atoms	Microwave counts	Laser counts	Counts upon release
1	Single	$1S_{cd} \rightarrow 2P_{c\pm}$	4	600	12	24,000	2,004	-	1,197	807
2	Single	$1S_{cd} \rightarrow 2P_{f\pm}$	4	550	12	24,000	2,012	-	1,075	937
3	Double	$1S_{d} \rightarrow 2P_{c-}$	2	440	12	12,000	1,044	527	229	288
4	Double	$1S_{d} \rightarrow 2P_{f-}$	2	720	12	12,000	971	463	341	167

Table 2: 1*S*-2*P* transition frequencies.

The experimentally determined transition frequencies for antihydrogen f_{res}(exp) (with 1-s.d. errors in parentheses) are compared with the theoretically expected values for normal hydrogen f_{res}(th), at a magnetic field of 1.0329 T. For the singly spin-polarized experiments, the centroid of the hyperfine states is given. The transition frequencies for normal hydrogen were calculated to a precision better than 1 MHz (Methods).

	Sample spin polarization	Antihydrogen f_{res}(exp) (MHz)	Normal hydrogen f_{res}(th) (MHz)	Difference f_{res}(exp)- f_{res}(th) (MHz)
$1S_{cd} \rightarrow 2P_{c\pm}$	Single	2466051659(62)	2466051625	34
$1S_{cd} \rightarrow 2P_{f\pm}$	Single	2466036611(88)	2466036642	-31

$1S_d \rightarrow 2P_{c-}$	Double	2466051189(76)	2466051270	-81
$1S_d \rightarrow 2P_{f-}$	Double	2466036395(81)	2466036287	108

Table 3: Summary of the uncertainties.

Estimated uncertainties (1-s.d.) at 121.6 nm for each transition are tabulated (Methods).

Source of uncertainty	$1S_d \rightarrow 2P_{c-}$ Doubly spin-polarized (MHz)	$1S_d \rightarrow 2P_{f-}$ Doubly spin-polarized (MHz)	$1S_{cd} \rightarrow 2P_{c\pm}$ Singly spin- polarize (MHz)	$1S_{cd} \rightarrow 2P_{f\pm}$ Singly spin-polarized (MHz)
Lineshape fit statistics	55	54	45	47
Fit model dependence	24	42	17	62
Wavemeter drift	30	30	30	30
Wavemeter offset	18	18	18	18
730 nm cavity frequency correction	18	18	18	18
Residual $1S_c$ state atoms in doubly spin-polarized sample	23	16	0	0
Magnetic field	5	8	5	8
Total	76	81	62	88

Methods

Transition frequency determination

The observed 1*S*-2*P* transition spectra have asymmetric shapes with a low frequency tail caused by Zeeman shifts in the inhomogeneous magnetic field regions away from the centre of the ALPHA-2 trap. As a result, the apparent peak of the observed spectrum is shifted to a slightly lower frequency with respect to the resonant transition frequency f_{res}, which is defined for atoms in resonance at the magnetic field minimum of the trap. This offset is relatively small (order 50 MHz). Nonetheless, we performed extensive analysis to understand the effects of this asymmetry on our transition frequency determination. The details of the analysis follow.

A detailed simulation was used to model the motion of trapped antihydrogen atoms in the ALPHA-2 trap, as well as their interaction with pulsed laser radiation. Aspects of our simulation have been validated in previous studies (e.g. [10, 11, 19-24]). In order to determine the resonant transition frequency, we first simulated lineshapes for the transitions from the two trappable 1*S* hyperfine states to the $2P_c$ and $2P_f$ excited states (i.e. for a total of four transitions: $1S_c \rightarrow 2P_{c+}$, $1S_c \rightarrow 2P_{f+}$ $1S_d \rightarrow 2P_{c-}$, and $1S_d \rightarrow 2P_{f-}$). We then fit each component with an asymmetric lineshape function (referred to as *GE*). *GE* is a Gaussian spliced to an exponential low frequency tail, where the derivative of the crossover point is required to be continuous. *GE* has 4 parameters: the peak frequency (f_{peak}) and the width (W) of the Gaussian, the crossover point frequency (f_x), and the overall amplitude (A). From the fit, we determined the simulated lineshape parameters: $f_{peak}(sim)$, $W(sim)$, f_x (sim) and $A(sim)$ for each transition. In addition, we derived the peak frequency offset Δf, defined as $\Delta f = f_{peak}(sim) - f_{res}(th)$, where $f_{res}(th)$ is the expected theoretical resonance frequency for hydrogen in the magnetic field B.

The experimentally observed spectra were then fit with *GE* lineshapes. A sum of two *GE*s was used to fit singly spin-polarized samples, where only f_{peak}, and a single normalization factor were used as the fitting parameters, while the rest of the parameters, *i.e.* W and f_x of each *GE*, the spacing of f_{peak} between two *GE*s, and the ratio of the amplitude A of two *GE*s, were fixed to the corresponding simulated values. For doubly spin-polarized samples, the experimental spectra were fit with a single *GE* lineshape. In these fits, W and f_x were fixed from a fit to the simulated spectrum in which an estimated 5% contamination of $1S_c$ component was assumed. The experimental transition frequency is given by: $f_{\mathrm{res}}(exp) = f_{peak}(exp) - \Delta f$, where $f_{peak}(exp)$ is the peak frequency of the experimental data obtained by the fit. Here Δf corrects for the asymmetric lineshape as described earlier. The red lines (labeled as Model 1) in Fig. 3 show the results of these fits based on the standard simulations. Note that the transition to the $2P_e$ state is allowed when the laser polarization is not perfectly perpendicular to the B field. This could arise from the slight angle between the laser and the magnetic field (maximum 4 degrees at the edge of our trap), or the possible non-linear component in the polarization of the 121 nm light (expected to be order 10% or less). The frequency of the 1S-$2P_e$ transition is well separated from the 1S-$2P_c$ transition (by about -3.5 GHz), and its predicted intensity is very small (less than a few per cent of that for the 1S-$2P_c$ transition), hence it was ignored in the analysis.

Transition frequency uncertainties

Extensive studies have been performed to quantify the uncertainties in our frequency determination. The standard simulated spectra reproduce the observed lineshape reasonably well without any fine-tuning (Extended Data Fig. 1). The sensitivity of the obtained resonance frequency $f_{res}(exp)$ to the input parameters in the simulation was studied by varying these input parameters and repeating the same analysis.

The standard input to the simulation, and the range of the parameters studied (given in parentheses), were as follows. Laser pulse energies: 500 (350, 800) pJ; laser line linewidth 65 (50, 80) MHz; the relative magnitude of the laser sideband (present at +90 MHz with respect to the main band due to multimode lasing in the 730 nm amplification cavity): 10 (0, 25) %; the radial position displacement of the laser beam: 0 (0, 3) mm; the initial quantum state of antihydrogen at formation: n=30 (1, 30); the initial diameter of the cloud of antihydrogen: 0.45 (0.45, 0.90) mm; the temperature of antihydrogen at formation (before trapping): 15 (1, 15) K.

An alternative fit method was also used to study the robustness of our procedure. Here, the lineshape function *GE* was fit to the data without using constraints from the simulated spectrum. From the fit, $f_{peak}(exp)$ was extracted for each transition, and the experimental resonance frequency was determined as $f_{res}(exp) = f_{peak}(exp) - \Delta f$, where the offset Δf from the standard simulation was assumed. The lineshapes given by these fits are shown by blue lines (labeled as Model 2) in Fig. 3.

The results of the analyses using the simulations with varied input parameters, as well as alternative fit models, are given by red lines in Extended Data Fig. 1, which illustrate that the dependence on the details of fit procedure is small. The variations of the extracted frequency $f_{res}(exp)$ in these studies (both with different simulation input and different fit methods) were generally within the statistical uncertainties of these fits. We have taken the largest deviations in $f_{res}(exp)$ among these studies as a measure of the "fit model dependence" (Table 3).

It should be noted that our evaluation of fit model dependence systematics relies on the GE model being reasonable representation of the simulated data. This agreement was qualitatively illustrated in Extended Data Figure 1. Quantitatively, with the simulations with the standard input parameters, the chi-square per degree of freedom (DOF) ranges from 1.2 to 2.5 (with an average of 1.8), where DOF = 8. When the input parameters are varied, the chi-square per DOF ranges from 1.0 to 3.9, with an average of 2.1. The simulation statistics was roughly a factor of 2 to 4 greater than the data, hence these are reasonable values for our purpose.

The sources of uncertainty in transition frequencies can be summarized as follows (note that the frequency uncertainties at 730 nm should be multiplied by a factor of 6 to give those at 121 nm): (a) Wavemeter drift: this is due to temperature-induced drift of the wavemeter readings, which was estimated from offline studies to be about 20 MHz per degree at 730 nm. Given the recorded temperature variation of ±0.25 degree, we assigned an error of ±5 MHz at 730 nm. Note that a temperature drift during our 2-hour measurements would result in a broadening of the observed linewidth. This effect would be also taken into account partly by the fit model uncertainty discussed above. So, there is a possibly of partial double counting, but we conservatively list both effects separately. (b) Wavemeter offset: an offset of the He-Ne laser calibration source, estimated to be ±3 MHz at 730 nm by offline calibration.

(c) 730 nm cavity resonance frequency correction: the frequency of the generated 730 nm pulse was measured to be shifted from that of the cw 730 nm seed laser. This shift of about 10 MHz at 730 nm was regularly monitored, and was corrected for in our frequency determination. We conservatively assign an error in this correction as 10/sqrt(12) = 3 MHz at 730 nm (the standard deviation of a uniform distribution with a width of 10 MHz). (d) Residual $1S_c$ state contamination: our earlier studies with shorter running times [11, 22] indicate there is a residual population of order 5% of the $1S_c$ state after the microwave-driven clearing procedure, which was corrected for in the analysis above. We estimate the error in this correction by analyzing the data assuming no residual $1S_c$ population. We take 68% of the differences between the two analyses (33.5 MHz and 24 MHz for the $2P_c$ and $2P_f$ transitions) as one sigma uncertainties in the correction. (e) Magnetic field: the field at the magnetic minimum of the ALPHA-2 trap was measured in situ via the electron cyclotron resonance method [34]. A conservative uncertainty of 10 MHz in the ECR measurement gives a B field error of 3.6 x 10^{-4} T, which in turn gives frequency errors of 5 and 8 MHz for the $1S$-$2P_c$ and $1S$-$2P_f$ transitions at 1 T. We take these values as a measure of uncertainty due both to the absolute value and to the run-to-run stability of the B field. Note that frequency uncertainty in the $1S$-$2S$ transition due to B field variations is negligible for our purposes [11]. (f) Fit statistical uncertainties: these represent statistical uncertainties in the fit both from the experimental data and the simulations. (g) Model uncertainties: described above.

The total errors for each transition are given by a quadratic sum of the errors (a) to (g). Care has to be taken when taking an averaging or a difference of the transition frequencies. Here, we assumed that error (b), the wavemeter offset, introduces a common offset to all the series. The other errors are assumed to be uncorrelated across the data set. The resulting combined uncertainty for the transition frequencies of antihydrogen is 39 MHz, or 16 parts per billion (Fig. 4, average value). We expect that virtually all of the uncertainties can be significantly reduced in the near future with the increased statistics and by improved control of the systematics.

Determination of the fine structure splitting and the Lamb shift of antihydrogen

In order to analyze the Zeeman shifted energy levels of antihydrogen in the $2P$ state, we used the following Hamiltonian for the $2P$ state, which includes the field-free Hamiltonian ($\hat{H}_0$), the fine structure Hamiltonian ($\hat{H}_{FS}$), the Zeeman Hamiltonian ($\hat{H}_Z$), and the fine structure Hamiltonian ($\hat{H}_{hf}$);

$$\hat{H} = \hat{H}_0 + \hat{H}_{FS} + \hat{H}_Z + \hat{H}_{hf} \quad \text{(eq. 1)}$$

$$\hat{H}_{FS} = \frac{2}{3}\overline{\mathcal{E}}_{FS}\left[\frac{1}{\hbar^2}\vec{L}_{\overline{e}}\cdot\vec{S}_{\overline{e}} + 1\right], \quad \text{(eq. 2)}$$

$$\hat{H}_Z = -\frac{2\mu_{\overline{e}}(2P)}{\hbar}\vec{S}_{\overline{e}}\cdot B - \frac{2\mu_{\overline{p}}}{\hbar}\vec{I}_{\overline{p}}\cdot\vec{B} + \frac{\tilde{\mu}_{\overline{B}}}{\hbar}\vec{L}_{\overline{e}}\cdot\vec{B} \quad \text{(eq. 3)}$$

$$\hat{H}_{hf} = \frac{\overline{C}_{IL}}{\hbar^2}\vec{I}_{\overline{p}}\cdot\vec{L}_{\overline{e}} + \frac{\overline{C}_{IS}}{\hbar^2}\left[\vec{I}_{\overline{p}}\cdot\vec{S}_{\overline{e}} - 3(\vec{I}_{\overline{p}}\cdot\vec{r})(\vec{S}_{\overline{e}}\cdot\vec{r})\right]. \quad \text{(eq. 4)}$$

Here, $\vec{L}_{\overline{e}}$ is the orbital angular momentum of the positron, $\vec{S}_{\overline{e}}$ is the positron spin angular momentum, $\vec{I}_{\overline{p}}$ is the antiproton nuclear spin angular momentum and $\vec{r}$ is the

position vector of the positron. $\overline{\mathcal{E}}_{FS}$ is the fine structure splitting of antihydrogen at the zero field. The magnetic moments of positron and antiproton are given by $\mu_{\overline{e}}(2P) = \frac{|\overline{g}_s|}{2}\frac{|\overline{e}|\hbar}{2m_{\overline{e}}}\left(1-\frac{\alpha^2}{10}\right)$ and $\mu_{\overline{p}} = -\frac{|\overline{g}_p|}{2}\frac{|\overline{e}|\hbar}{2m_{\overline{p}}}$ where $\overline{g}_s$ and $\overline{g}_p$ are the positron spin and antiproton g-factors, $\overline{e}$and $m_{\overline{e}}$ are the charge an mass of the positron, and α is the fine structure constant. The last term of Eq. 4 is the Zeeman interaction due to the orbital angular momentum of the positron with the magnetic moment of $\tilde{\mu}_{\overline{B}} = -\left(1-\frac{m_{\overline{e}}}{m_{\overline{p}}}\right)\frac{|\overline{e}|\hbar}{2m_{\overline{e}}}$ where $m_{\overline{p}}$ is the mass of the antiproton. $\overline{C}_{IL}$ is the hyperfine coupling constant due to the antiproton spin and the orbital angular momentum of the positron, and $\overline{C}_{IS}$ is the hyperfine interaction due to the magnetic dipole-dipole interaction.

For the analysis of the Lamb shift ($\overline{\mathcal{E}}_{Lamb}$) and the fine structure parameter ($\overline{\mathcal{E}}_{FS}$) of antihydrogen, we assumed that the absolute values of the three magnetic moments ($\mu_{\overline{e}}$, $\mu_{\overline{p}}$, and $\mu_{\overline{B}}$) are the same as those of normal hydrogen. Previous measurements of basic properties of antiparticles are consistent with this assumption. The hyperfine coupling constants are also assumed to be those of normal hydrogen, whose values are $\overline{C}_{LI}$= 22.2 MHz and $\overline{C}_{SI}$ = -22.2 MHz taken from normal hydrogen [37].

Our measurements determine the energy levels, with respect to the 1*S* ground state, of two of the Zeeman sub-levels in the *n=2* positronic manifold of antihydrogen at a magnetic field of 1.0329 T. Specifically, the $2P_f$ state belongs to the $2P_{1/2}$ manifold, and the $2P_c$ state belongs to the $2P_{3/2}$ manifold (see Fig. 1). We combine these results with our previous measurement of the $1S_d$-$2S_d$ level [7], and assume validity of the standard Zeeman and hyperfine interaction in order to derive the fine structure splitting $\overline{\mathcal{E}}_{FS}$ (*i.e.*, the $2P_{1/2} - 2P_{3/2}$ energy difference), and the Lamb shift $\overline{\mathcal{E}}_{Lamb}$ (*i.e.*, the $2S_{1/2} - 2P_{1/2}$ energy difference), both defined at zero field.

Taking into account the hyperfine splitting, we find the energy separation between the $2P_{c-}$ and $2P_{f-}$ levels at 1.0329 T to be 14.945 ±0.0975 GHz from the difference of the weighted average values of the observed transition frequencies. Furthermore, we obtain the separation between $2S_d$ and $2P_{c-}$ levels to be $\Delta E(2S, 2P_c)$ = 9,832 ± 49 MHz, and that between the $2S_d$ and $2P_{f-}$ levels to be $\Delta E(2S, 2P_f)$ = 24,778 ± 60 MHz, at the same field. The sum and the difference of the two quantities, $\Delta E(2S, 2P_c)$ and $\Delta E(2S, 2P_f)$, can be expressed as the following equations, based on the standard Hamiltonian of the hydrogen atom in a magnetic field *B* [35, 36]. We neglect terms that contribute less than 1 MHz.

$$\Delta E(2S,2P_f) - \Delta E(2S,2P_c) = 2E_1(-B) + \frac{1}{2}\overline{C}_{LI}\cos 2\sigma + \frac{1}{10}\left(\cos 2\sigma - 3\sqrt{2}\sin 2\sigma\right)\overline{C}_{SI} \quad \text{(eq.5)}$$

$$\Delta E(2S,2P_f) + \Delta E(2S,2P_c) = 2\overline{\mathcal{E}}_{Lamb} - \overline{\mathcal{E}}_{FS} + \frac{1}{2}\overline{C}_{LI} - \frac{3}{10}\overline{C}_{SI} + \frac{1}{2}\overline{\mathcal{E}}_{HF}(2S) - (2\mu_{\overline{e}}(2P) + \tilde{\mu}_{\overline{B}})B \quad \text{(eq.6)}$$

where

$$E_1(-B) = \sqrt{\left\{\frac{1}{6}\overline{\mathcal{E}}_{FS} - B\left(\mu_{\overline{e}}(2P) + \frac{1}{2}\tilde{\mu}_{\overline{B}}\right)\right\}^2 + \frac{2}{9}\overline{\mathcal{E}}_{FS}^2},$$

and

$$\tan\sigma = \frac{-\overline{\mathcal{E}}_{FS} + \{6\mu_{\bar{e}}(2P) + 3\tilde{\mu}_{\overline{B}}\}\, B + 6E_1(-B)}{2\sqrt{2}\;\overline{\mathcal{E}}_{FS}}\,.$$

Here, $\overline{\mathcal{E}}_{HF(2S)}$ is the hyperfine splitting in the 2*S* state at zero field.

Finally, using the CODATA 2014 values of the fundamental constants for the normal hydrogen atom [38], the fine structure splitting $\mathcal{E}_{FS}$, and the Lamb shift, $\mathcal{E}_{Lamb}$, of the antihydrogen atom are determined by numerically solving equations 5 and 6 with the measured energy level differences given in Table 2 as input.

Normal hydrogen transition frequencies in a magnetic field

From the measurements in normal hydrogen at zero field for the $1S_{1/2}$ - $2S_{1/2}$ transition [39], $2S_{1/2}$ - $2P_{1/2}$ [40], and $2P_{1/2}$ - $2P_{3/2}$ [41], we obtain hyperfine centroid frequencies of:

$1S$ -$2P_{1/2}$ transition: 2,466,060,355 MHz,
$1S$ -$2P_{3/2}$ transition: 2,466,071,324 MHz.

The transition frequencies at 1.0329 T (Table 2) are calculated by evaluating corrections based on the standard Zeeman, fine structure and hyperfine interactions in a magnetic field [35, 36], and using the current CODATA values of the fundamental constants [38]. The precision of our calculations is better than 1 MHz.

In comparing the normal hydrogen values with the measured antihydrogen frequencies in Table 2 and in Fig. 4, the value of the magnetic field was assumed to be exact for normal hydrogen case.

References:

[34] Amole, C. et al. *In situ* electromagnetic field diagnostics with an electron plasma in a Penning–Malmberg trap. *New J. Phys.* **16**, 013037 (2014).
[35] Rasmussen,C Ø, Madsen, N., Robicheaux, F. Aspects of 1S-2S spectroscopy of trapped antihydrogen atoms, *J. Phys.* B **50**, 184002 (2017).
[36] Melezhik,V. S., Schmelcher, P. Quantum energy flow in atomic ions moving in magnetic fields, *Phys. Rev. Lett*. **84**, 1870-1873 (2000).
[37] Kramida, A.E. A critical compilation of experimental data on spectral lines and energy levels of hydrogen, deuterium, and tritium. *At. Data Nucl. Data Tables* **96**, 586–644 (2010).
[38] Mohr, P. J., Newell, D. B., Taylor, B. N. CODATA recommended values of the fundamental physical constants: 2014. *Rev. Mod. Phys*. **88**, 035009 (2016).
[39] Parthey, C. G. et al. Improved measurement of the hydrogen 1S–2S transition frequency. *Phys. Rev. Lett.* **107**, 203001 (2011).
[40] Lundeen, S. R. & Pipkin, F. M. Measurement of the Lamb shift in hydrogen n=2. P*hys. Rev. Lett*. **46**, 232-235 (1981).
[41] Hagley, E. W. and Pipkin, F. M. Separated oscillatory field measurement of hydrogen $2S_{½}$ - $2P_{3/2}$ fine structure interval. *Phys. Rev. Lett.* **72**, 1172-1175 (1994).

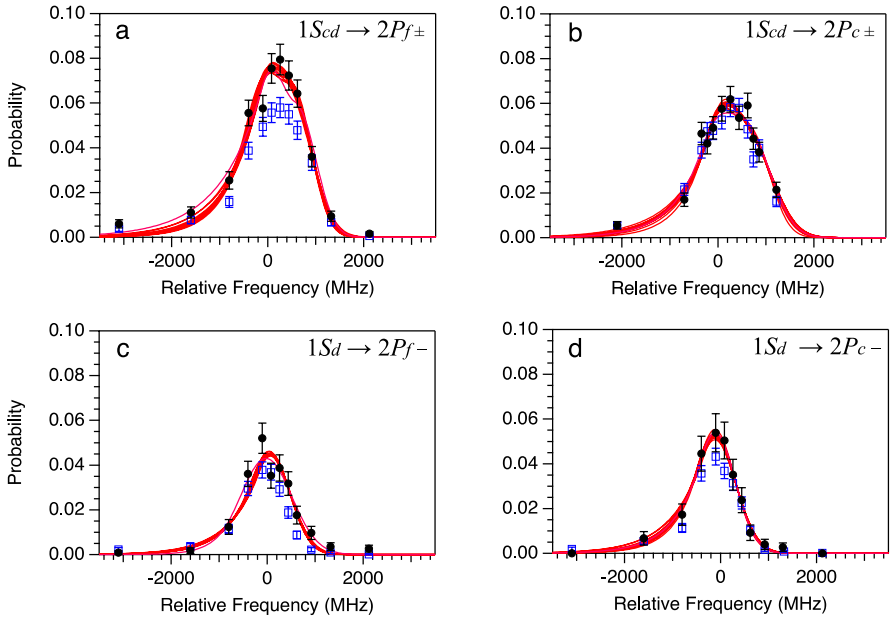

Extended Data Figure 1: Systematic studies for the determination of transition frequencies.

For each series, the experimental data (filled black circles with error bars) are plotted with fits of various models, where each of the red curves represents one of the models discussed in Methods. The experimental data points are normalized to the total number of the detected antihydrogen atoms and a laser power of 5 nW. Also shown are the standard simulations, similarly normalized to the total number of simulations atoms (open blue squares with error bars), which illustrate the degree of agreement between the data and the simulations without any tuning parameters. Some discrepancies in the amplitudes can be observed, which may point to the errors in our laser power estimates. Note that our frequency fit procedure allows variations in the

relative amplitudes, hence are largely insensitive to the amplitude differences (Methods).